

Valence band offset, strain and shape effects on confined states in self-assembled InAs/InP and InAs/GaAs quantum dots

M. Zieliński*

Instytut Fizyki UMK, Grudziądzka 5, 87-100 Toruń, Poland

Abstract

I present a systematic study of self-assembled InAs/InP and InAs/GaAs quantum dots single particle and many body properties as a function of quantum dot-surrounding matrix valence band offset. I use an atomistic, empirical tight-binding approach and perform numerically demanding calculations for half-million atom nanosystems. I demonstrate that the overall confinement in quantum dots is a nontrivial interplay of two key factors: strain effects and the valence band offset. I show that strain effects determine both the peculiar structure of confined hole states of lens type InAs/GaAs quantum dots and the characteristic „shell-like” structure of confined holes states in commonly considered ”low-strain” lens type InAs/InP quantum dot. I also demonstrate that strain leads to single band-like behavior of hole states of disc type („indium flushed”) InAs/GaAs and InAs/InP quantum dots. I show how strain and valence band offset affect quantum dot many-body properties: the excitonic fine structure, an important factor for efficient entangled photon pair generation, and the biexciton and charged excitons binding energies.

I. INTRODUCTION

Fully ab-initio, parameters free, modeling of million atom self-assembled¹ or nanowire² quantum dots (QDs) is still beyond the reach of current computers. For practical, atomistic calculation, semi-empirical approaches like the empirical tight-binding (ETB)³⁻¹⁶ or the empirical pseudopotential method (EPM)¹⁷⁻²⁴ are typically employed. The calculation scheme usually starts with strain field calculation followed by the single particle calculation followed then with the configuration interaction approach to obtain many-body (exciton, charged exciton, multi-exciton) spectra^{12,13}.

Semi-empirical approaches use sets of fitted parameters determined to reproduce bulk properties like effective masses, bulk deformation potentials and gaps at different points of the Brillouin zone²⁵. Bulk derived parameters are later used for calculation of nanosize systems. Apart from potential („bulk to nanosystem”) transferability issues, one may question the reliability of important parameters describing bulk electronic structure, that act as the input data for the empirical fitting procedure. For example, in the case of the absolute InAs valence band deformation potential (a_v) not even the sign of this quantity is unambiguously determined²⁶⁻³³. As semiconductor (self-assembled or nanowire) quantum dots are typically mixed material systems an additional empirical bulk parameter, the valence band offset between quantum dot and surrounding matrix material, has to be incorporated into the Hamiltonian. This „natural”^{33,34} valence band offset (VBO) determines the depth of unstrained hole and electron confining potentials and combined with strain and deformation potentials constitutes the overall confining potential for the strained case, i.e. the „strained” band offset. There is again a substantial uncertainty of the natural VBO values, e.g., the reported InAs/GaAs VBO varies from 50 meV to 500 meV^{26,34}. The source of this discrepancy is not only due to the difference between experimentally and theoretically reported values, but³³: ”It is to be emphasized, however, that even within the framework of Kohn-Sham DFT, different computational schemes result in different predictions for the natural band offsets [...]”. Y.H. Li and co-workers³⁴ state additionally that there has been ”long-standing anomalies between theory and experiment” and in their ab-initio calculation ”For GaAs/InAs the predicted offset is increased from 0.06 eV in the previous calculation to 0.50 eV”.

For a given pair of materials (e.g. InAs/GaAs) the VBO has only one value, however

as discussed above, this value is practically unknown or given with large (> 100 meV) uncertainty. E.g. the $VBO=0.06$ eV is used in the EPM approach, the $VBO\approx 0.17$ eV is utilized in $\mathbf{k}\cdot\mathbf{p}$ studies³⁵, the $VBO=0.23$ eV is incorporated in the ETB model by Boykin et al.³⁶, while $VBO\approx 500$ meV is reported by the DFT calculations³⁴. In this work, as practical resolution of this problem, I utilize an approach in which I perform calculations by an artificial variation of the VBO over wide range of values. While the VBO has been considered as a merely technological parameter of lesser importance, the current study shows that it is quite the opposite. Both the single particle and the many body properties are affected by the choice of the VBO and the caution should be exercised before applying different VBO values in the semi empirical calculation. Abstracting from the experimental reality (there is only one, yet unknown VBO value, for a given pair of materials), the "artificial" modification of the VBO is by itself a very interesting theoretical tool to study the effects of band confinement versus other effects such as strain. For example, the calculation of spectra for InAs/InP and InAs/GaAs lens type quantum dots using the same (yet artificial) VBO helps to understand the difference between both types of nanosystems.

The ambiguity of the a_v and VBO bulk material values may thus affect¹⁴ the accuracy of the qualitative description of confined valence band states in semiconductor nanosystems. This is further important as recent empirical pseudopotential method works (e.g. Refs.²³ or⁴⁴ etc.) still refer to older EPM parameterizations²² utilizing the "questioned"³⁴ VBO value ≈ 50 meV. The Section E of the paper discusses this point showing that while 'natural' VBOs in ETB and EPM can differ significantly, the strained band offsets in two approaches are very similar.

Despite over a decade of intensive studies the problem of detailed understanding of holes in self-assembled InAs quantum dots is still an active field of research³⁷. Ediger et al.³⁸ observed characteristic spectral structure of hole states in InAs/GaAs lens type quantum dots leading to a non trivial hole charging pattern of excitonic complexes. In our earlier work¹¹ we have noticed that InAs/GaAs quantum dot shape affects spectral properties of holes significantly. Recently Gong et al.^{23,24} have calculated electronic structure of InAs/InP lens type quantum dot and speculated that differences with respect to analogous InAs/GaAs system is due to different common ion or different VBO in both systems. In this work, by the systematic VBO analysis, I show it is not the VBO, but rather strain effects that play a dominant role in determining the character of single particle holes states in quantum dots.

A two photon cascade from the QD biexciton state can generate entangled photons³⁹ and has attracted great interest for applications in quantum information. However, anisotropic exchange splitting of quantum dot bright excitons, induced by the asymmetry of typical quantum dots, inhibits entanglement. Understanding the origins of fine structure splitting is thus of great importance for potential quantum dot applications. Recently, yet another scheme for entangled photons generation has been proposed^{40–42}, in which the biexciton binding energy is tuned to zero. As in a typical experiment different excitonic complexes (both charged and neutral) are observed together, the prediction of the spectral line order²⁴ or binding energies is usually far from trivial. To solve such issues, an inverse approach for quantum dot calculation has been recently proposed⁴³. In this method one uses excitonic spectroscopy experimental data to determine quantum dot structural properties. However the accuracy of such prediction must depend on the accuracy of the many-body calculations and indirectly on empirical parameters (such as the VBO) used in a calculation.

In this work I compare properties of strained and unstrained systems, study the role of quantum dot shape and the evolution of single particle and charge probability densities as a function of valence band offset. By a systematic VBO analysis, I show that strain and valence band offset effects play different, important roles in determining the character of single particle states in quantum dots. Finally, I show that the choice of VBO affects substantially many body energies, in particular biexciton and trions binding energies and the excitonic fine structure.

II. SYSTEMS AND METHODS

In the following I present a systematic study of lens and disc type InAs quantum dots, surrounded by either InP or GaAs, as a function of valence band offset, with strain effects included or artificially neglected. The height of the disc type quantum dot is $h = 3$ nm and the base diameter is $D = 16.8$ nm. For the sake of comparison with the EPM calculations^{21–24} the height of the lens type dot is chosen as $h = 3.5$ nm and the base diameter is $D = 25$ nm. Both dots are located on 1 nm thick wetting layer. The presence of the wetting layer is particularly important for disc type quantum dots as it lowers the overall quantum dot symmetry from D_{2d} to C_{2v} (the lack of "rotoinversion operation"⁴⁴) and therefore both kinds (lens and disc) of quantum dots have low C_{2v} symmetry.

The calculation consists of several major steps: first atomic positions are calculated. There is a lattice mismatch between dot material (InAs) and surrounding matrix material (GaAs or InP). To calculate strain relaxed positions I use the atomistic valence force field (VFF) approach of Keating⁴⁵. This method is described in more detail in ref.^{46,47} and in our previous works^{10,12}. The size of the computational domain, including more than 50 million atoms, guarantees convergence of the strain distribution⁴⁸.

Due to small lattice mismatch of InAs and InP I neglect the piezoelectric effects in the present calculation, following similar arguments by Gong et al.²³ who ignore piezoelectricity in the empirical pseudopotential work on InAs/InP quantum dots. Consistently, piezoelectric effects can also be neglected for low aspect ratio^{7,8,35} lens and disc type InAs/GaAs quantum dots, where the piezoelectricity is either negligible²⁰ or the contribution due to second-order effects tends to cancel linear terms^{35,49}. In particular for lens type InAs/GaAs ref.³⁵ states that: "for smaller aspect ratios [...] first- and second-order effects compensate each other with respect to their impact on the electronic states." Finally the piezoelectricity is neglected for a sake of a fair comparison with other approaches where this effect is neglected (comment 41 from ref.²¹).

In the second step of the calculation, the single particle states are obtained by building the $sp^3d^5s^*$ tight-binding Hamiltonian^{14,25} and then diagonalizing the Hamiltonian by means of the Arnoldi algorithm with the matrix-vector multiplication parallelized using *OpenMP* approach on 48 core, shared memory system.

The single-particle tight-binding Hamiltonian for the system of N atoms and m orbitals per atom can be written in the language of the second quantization (in the site basis) in the following form:

$$\hat{H}_{TB} = \sum_{i=1}^N \sum_{\alpha=1}^m E_{i\alpha} c_{i\alpha}^+ c_{i\alpha} + \sum_{i=1}^N \sum_{\alpha=1, \beta=1}^m \lambda_{i\alpha, \beta} c_{i\alpha}^+ c_{i\beta} + \sum_{i=1}^N \sum_{j=1}^4 \sum_{\alpha, \beta=1}^m t_{i\alpha, j\beta} c_{i\alpha}^+ c_{j\beta} \quad (1)$$

where $c_{i\alpha}^+$ ($c_{i\alpha}$) is the creation (annihilation) operator of a carrier on the orbital α localized on the site i , $E_{i\alpha}$ is the corresponding on-site (diagonal) energy, and $t_{i\alpha, j\beta}$ describes the hopping (off-site, off-diagonal) of the particle between orbitals on (4) nearest neighboring sites. Coupling to further neighbors is neglected. Finally, $\lambda_{i\alpha, \beta}$ (on-site, off-diagonal) accounts for the spin-orbit interaction following the description given by Chadi⁵⁰.

As QD/matrix material lattice constants do not enter TB Hamiltonian explicitly strain in the TB method is accounted by the modification of Hamiltonian matrix elements from bulk

(unstrained) values to values modified due to bond lengths/angles modification. Therefore if one uses InAs/(GaAs,InP) bulk Hamiltonian matrix elements, one is simply neglecting strain effects. Therefore for the (artificially) unstrained¹⁰ systems I use bulk TB parameters set from Ref.²⁵ and thus there is no strain contribution in the Hamiltonian nor the relaxation of atomic position is accounted for. In other words the "unstrained" system ("strain effects neglected") corresponds to strain "unrelaxed" system with the VFF step and modification of TB parameters neglected. For the strained systems, since strain effects change bond lengths and angles, strain relaxed positions are used to modify TB parameters (diagonal and off-diagonal matrix elements) following the description given in detail in my earlier work¹⁴.

I have calculated the single particle spectra for many VBO values from 50 meV to 500 meV with 10 meV step. In this work I use a multi-scale (multi-domain) approach where smaller computational domain is used for the single particle calculation^{48,51}. Yet, as the number of atoms in the TB domain is larger than half a million, in order to make the entire process feasible I calculate only eigenenergies of several lowest electron and holes confined states. Then for several chosen VBO values I additionally calculate eigenstates and plot corresponding probability charge densities.

Finally, for several VBO values electron and hole Coulomb matrix elements (Coulomb direct and exchange integrals) are calculated according to the approach given in ref.¹². In a GW approach⁵² one calculates the effective interaction W self-consistently. Not being able to carry out this calculation, we assume a statically screened Coulomb interaction. Hence the Coulomb matrix elements V_{ijkl} are given by:

$$V_{ijkl} = \int \int \phi_i^*(\vec{r}_1) \phi_j^*(\vec{r}_2) \frac{e^2}{\epsilon(\vec{r}_1, \vec{r}_2) |\vec{r}_1 - \vec{r}_2|} \phi_k(\vec{r}_2) \phi_l(\vec{r}_1) \quad (2)$$

where $\epsilon(\vec{r}_1, \vec{r}_2)$ is the position-dependent dielectric function and ϕ are single-particle wave functions. By substituting single-particle wave functions in the form of linear combination of atomic orbitals: $\phi_i = \sum_{\vec{R}, \alpha} b_{\vec{R}\alpha}^i |\vec{R}\alpha\rangle$ into Eq. 2 and then by utilizing a series of approximations^{3,12} (including the two-center approximation and accounting for monopole-monopole contributions only) one obtains an approximate form of Coulomb ma-

trix elements¹²:

$$\begin{aligned}
V_{ijkl} = & \sum_{\vec{R}_1} \sum_{\vec{R}_2 \neq \vec{R}_1} \left[\sum_{\alpha_1} b_{\vec{R}_1 \alpha_1}^{i*} b_{\vec{R}_1 \alpha_1}^l \right] \left[\sum_{\alpha_2} b_{\vec{R}_2 \alpha_2}^{j*} b_{\vec{R}_2 \alpha_2}^k \right] \frac{e^2}{\epsilon |\vec{R}_1 - \vec{R}_2|} + \\
& \sum_{\vec{R}_1} \sum_{\alpha_1 \alpha_2 \alpha_3 \alpha_4} b_{\vec{R}_1 \alpha_1}^{i*} b_{\vec{R}_1 \alpha_2}^{j*} b_{\vec{R}_1 \alpha_3}^k b_{\vec{R}_1 \alpha_4}^l \langle \vec{R}_1 \alpha_1, \vec{R}_1 \alpha_2 \left| \frac{e^2}{|\vec{r}_1 - \vec{r}_2|} \right| \vec{R}_1 \alpha_3, \vec{R}_1 \alpha_4 \rangle. \quad (3)
\end{aligned}$$

The first term is the long-range, bulk-screened, contribution to the two-center integral built from the monopole interaction of two charge densities localized at different atomic sites. The second term is the on-site unscreened part, calculated by direct integration using atomic (Slater) orbitals^{4,5}. This approach is justified by the fact that the screening (Thomas-Fermi) radius ($\approx 2 - 4\text{\AA}$) is on the order of bond length^{4,51} resulting in nearly bulk screening of off-site (long-range) terms and limited screening of on-site (short-range) terms contribution.

The Hamiltonian for the interacting electrons and holes can be written in second quantization as:⁵³:

$$\begin{aligned}
\hat{H}_{ex} = & \sum_i E_i^e c_i^\dagger c_i + \sum_i E_i^h h_i^\dagger h_i + \frac{1}{2} \sum_{ijkl} V_{ijkl}^{ee} c_i^\dagger c_j^\dagger c_k c_l + \frac{1}{2} \sum_{ijkl} V_{ijkl}^{hh} h_i^\dagger h_j^\dagger h_k h_l \\
& - \sum_{ijkl} V_{ijkl}^{eh,dir} c_i^\dagger h_j^\dagger h_k c_l + \sum_{ijkl} V_{ijkl}^{eh,exchg} c_i^\dagger h_j^\dagger c_k h_l \quad (4)
\end{aligned}$$

The many-body Hamiltonian for the exciton (X), the biexciton (XX), positively (X^-) and negatively charged (X^+) trions is solved using the configuration interaction approach^{12,13}.

The quantum dot and the surrounding matrix may share the same anion (e.g. InAs/GaAs QD), cation (e.g. InAs/InP QD) or not have a common ion (e.g. InAs/GaP). In the empirical tight-binding the treatment of quantum dot/material interface atoms is ambiguous. In Boykin et al.³⁶ approach, this is handled during the fitting procedure where the diagonal Hamiltonian matrix elements of the common atom are kept the same in both materials. The value on the material band offset is incorporated into off-diagonal hopping matrix elements. This approach removes the necessity of modifying on-site matrix elements for interface atoms, but complicates significantly for ternary systems like InAs/InP/GaP, where, e.g., the bulk GaP properties are indirectly coupled to InAs bulk properties through the fitting process. Additionally as VBOs are embedded into the tight-binding parameterization, a necessary, complicated refit would be needed for every different VBO values. In this work I use the approach¹⁴ in which I account for the valence band offset by shifting diagonal matrix elements of the quantum dot material. On-site matrix elements of interface atoms

are calculated as a weighed sums of neighboring atoms materials on-site parameters. The Hamiltonian is built and then diagonalized for each VBO value: this gives a capability of freely tuning VBO, suitable thus for the VBO dependence studies.

III. RESULTS

Figure 1 shows the evolution of single particle electron and hole energy levels for the lens type InAs/GaAs quantum dot as a function of the InAs/GaAs VBO. With the increasing VBO value there is an energy upshift due to overall „reference level” (VBO) energy shift, while the effective band gap $E_{gap} = e_1 - h_1$ does not change considerably^{9,10}. In this work I show that while the above statement is generally true^{9,10,54}, the situation is far more complicated for spectral quantities other E_{gap} . To analyze the specifics of electron and hole spectra in the following plots I subtract the corresponding carrier ground state energy as illustrated for example on Figure 1b) and 1c).

Valence band offset is related to (natural or unstrained) conduction band offset CBO through the following relation $CBO = matrix_{gap} - dot_{gap} - VBO$, where $matrix_{gap}$ is the bulk band gap of the matrix material (GaAs or InP) and dot_{gap} is bulk band gap of the quantum dot (InAs) material. For the VBO in 50 – 500meV range, the CBO varies correspondingly from $\sim 1\text{eV}$ to $\sim 0.5\text{eV}$, with little difference between InAs/GaAs and InAs/InP cases, due to 0.1 eV difference of InP and GaAs bulk band gaps. Increasing the VBO corresponds thus to decreasing of the CBO, i.e. lower confinement of electron states. Even though CBO is nominally larger than VBO, effects of CBO variation on electron states should be observable due to their lower confinement (effective mass).

Figure 2 and 3 show energy levels corresponding to several lowest electron (upper- CB) and hole (lower- VB) states calculated for InAs/InP and InAs/GaAs disc type and lens type quantum dots as function of quantum dot-matrix valence-band offset (VBO) with strain effects either artificially neglected or included. Figures from Figure 4 to Figure 10 show corresponding charge/probability density isosurfaces. These figures contain substantial amount of information and will be analyzed in detail in the following part of the text.

A. Electron states - strain effects neglected

In an artificially unstrained InAs/(InP,GaAs) disc type quantum dot energy spectra of lowest electron levels reveal shell like structure [Fig. 2 a) and b)], with the ground electron state of s character [Fig. 4]. Despite the absence of strain and the rotational shape symmetry of the disc quantum dot, the presence of atomistic interfaces and low symmetry of underlying crystal lattice introduces the asymmetry into the system Hamiltonian²⁰. Thus, there are two closely spaced (splitting $< 1.5\text{meV}$) excited states (e_2 and e_3) of p -like character (of approximate angular momentum character $L = \pm 1$), followed by two excited (e_4 and e_5) closely spaced states (splitting $\approx 4\text{ meV}$) of d -like character. Splittings within p and d shell are still however much smaller than spacings between different shells: $s - p$ (60 meV) and $p - d$ (70 meV). The e_6 (of "2s" character²⁰) is separated from the lower lying d -like states e_4, e_5 by $\approx 20\text{ meV}$, a hallmark of disc-like confinement¹. Such structure of levels with quasi-degenerate energies corresponding to $L = 0, \pm 1, \pm 2, \dots$ is to be expected for nominally cylindrical disc-shaped quantum dots.

Charge probability densities corresponding to several lowest electron states in an artificially unstrained InAs disc type quantum dot practically do not change in the considered range of VBO values and are very similar for both InP and GaAs matrices [Fig.4]. For small VBO $\approx 100\text{ meV}$ there is a slight elongation of the p -shell states (e_2 and e_3) along $[110]$ and $[\bar{1}\bar{1}0]$ crystal axis, but otherwise these states have well defined cylindrical-like symmetry. For the VBO changing from 0.1 eV to 0.4 eV, the corresponding ground electron state localization inside quantum dot drops only by 3%, i.e. from 81% to 78% in InAs/InP case and from 86% to 83% in InAs/GaAs case. With no strain effects included, the confinement is generally somewhat lower for InAs/InP systems due to lower InP band gap (and thus lower CBO) than for the InAs/GaAs case.

For the disc type quantum dot, in the absence of strain, spacings between different shells $s - p$ and $p - d$ do not change much as a function of VBO, however Figure 5 shows that the splitting of the p -shell („ p -shell anisotropy”) increases monotonically (quasi-parabolically) with decreasing confinement, most likely due to the increasing role of interface effects in progressively shallower (decreasing CBO) well for electrons. Notably, in the absence of strain, the p -shell splitting is systematically larger in disc type InAs/InP quantum dots than in disc type InAs/GaAs systems, which I speculate, can also be related to ($\approx 5\%$) lower

confinement of electrons in InAs/InP quantum dots. Another important difference between InAs/GaAs and InAs/InP systems is that in the first case the QD and the surrounding material share common anion (As), while in the latter case they share common cation (In). Since electron wave functions are more localized on cation sites, having quantum dot and matrix material with same cations will increase the amplitude of electron wave function at the interface, thus may increase the p-shell splitting for InAs/InP systems when strain effects are neglected.

In the effective mass approximation, lens type quantum dots are expected to show 2D harmonic oscillator-like spectrum^{1,55}. In my atomistic calculations for the lens type quantum dot [Fig. 3 a) and b)] I also observe the well pronounced shell structure of electrons levels and well defined nodal-structure of corresponding charge densities (Fig. 6). For the lens type quantum dot, electron $s - p$ and $p - d$ level spacings slightly decrease with the increasing VBO. The ground electron state charge distribution is apparently not affected by the choice of the matrix material. The lower electronic p-shell (e_2) state is localized along $[1\bar{1}0]$ crystal axes and the higher p-shell state is localized along $[110]$ axes for the InAs/GaAs system, while for the InAs/InP system both p-shell states maintain cylindrical-like symmetry. Figure 5 shows also that with strain effects neglected the p-shell splitting depends more strongly on the absolute depth of the confining potential due to the VBO rather than on the particular quantum dot shape. Higher lying states are approximately of the same symmetry for both GaAs and InP matrices (Fig. 6) with similar inter-shell spacings (≈ 60 meV).

B. Electron states - strain effects included

With the strained effects accounted for, the first important difference is a significant increase of the p-shell splitting for both disc and lens system (Figure 5) and the well pronounced elongation of the p-shell states along $[1\bar{1}0]$ and $[110]$ crystals axes (Figure 4). Interestingly the p-shell states elongation for the disc type quantum dots is opposite to that of the lens type quantum dots (Figure 6). Also, for the lens type quantum dot the orientation of the p-shell states is reversed²⁰ when compared to the strain-free case: the anisotropy due to atomic interface is thus reversed by the anisotropy due to strain. For the highly strained InAs/GaAs disc type quantum dot, the competition of two different anisotropy sources manifest itself by non-monotonic change of the p-shell splitting as a function of the

VBO (Figure 5). With strain effects included the p-shell splitting is generally higher for lens type than for disc type quantum dots, most likely due to larger surface(interface)/volume ratio in lens type systems. With strain effects neglected the p-shell splitting was generally larger for InAs/InP systems, however with strain effects included this trend reverses, the splitting is dominated by strain, and therefore is larger for InAs/GaAs than for InAs/InP systems. It is interesting to notice that while electron states are built predominately from s-type atomic orbitals (and thus should be affected predominantly by the non-directional hydrostatic strain) one expects non-zero electron-hole coupling⁵⁶ and thus one can speculate that the effects of (biaxial) strain on hole states (which will be discussed later) may also indirectly affect the electron p-shell splitting.

To summarize, the overall structure of p-shell electron states is thus determined by combined: matrix material, dot shape and VBO value and none of these factors can be neglected⁶⁵.

For confined quantum dot states (both electrons and holes) spacings between different shells (s-p, p-d, etc.) increase with the increasing confining potential depth (i.e. band offset, the CBO and the VBO for electron and holes correspondingly) as expected from the quantum confinement effect [Fig. 2 and Fig. 3]. However splitting of levels within a given shell decreases with the increasing confinement. This is due the progressively larger localization and effectively smaller influence of the material interface, which acts as the source of splitting. Consequently, higher lying (d-shell) states properties are even more susceptible to the choice of the VBO due to their lower confinement.

C. Hole states - strain effects neglected

Interestingly even when neglecting the strain effects, the ground hole state of the considered disc and lens type quantum dots has well defined s-like symmetry [Fig. 7 and Fig. 8] and is predominately of heavy-hole character. This initially may come as a surprise as in such case there are no heavy hole-light hole splitting terms due strain in the Hamiltonian⁵⁷. Yet, the quasi-two-dimensional confinement in flat quantum dot systems is efficient enough to separate both type of holes. Alternatively, one can associate heavy hole states with the in-plane component dominated by p_x and p_y atomic orbitals^{10,58} and affected by small, lateral confinement. Then the light-hole states are the predominantly constituted by p_z orbitals

and highly influenced by the vertical confinement, and thus energetically shifted away from the ground hole state.

Higher lying states however, for both types of quantum dots, reveal complex, mixed angular momentum character [Fig. 7 and Fig. 8] and show no clear shell-like structure of their energy spectra [Fig. 4 and Fig.6], that was so characteristic for the single-band-like confinement of electron states. For lens type dots, the first and the second excited hole states are not even of the p-like symmetry and no nodal planes are observed.

Due to strong ($> 90\%$) confinement of hole states in quantum dot area, with strain effects neglected, there is little difference between hole states properties with respect to the surrounding matrix (GaAs/InP). This is particularly true for large VBO values, and better confined states, where the interface effects play a lesser role. And consequently there is almost one to one correspondence of charge densities for the disc type InAs/InP and InAs/GaAs quantum dot cases (Figure 7).

Interestingly, even for the VBO= 0 eV and no strain effects included I still observe quantum dot hole confined states due to material property („effective mass”) discontinuity (Fig. 7).

D. Hole states - strain effects included

Strain affects holes states properties significantly. For disc type InAs/GaAs and InAs/InP quantum dots, in the „realistic”⁶⁶ range of VBO values (210 – 350 meV). the structure of confined hole states is in a vivid contrast to the strain-free case and resembles that of single-band electron confined states, with well pronounced shells of p-like and d-like symmetry. This effect is well visible, both in the charge distributions [Fig. 9] and in the energy spectra [Fig. 2 g) and h)]. The hole p-shell splitting lies within few meV, i.e. much smaller than (25 – 30 meV) s-p level spacing. Strain lifts heavy hole-light hole degeneracy^{46,57,58} and thus effectively decouples light-hole component of the confined hole function, leading to the single band-like behavior of hole states of disc type („indium flushed”⁵⁹) quantum dots and characteristic shell-structure know also from the experiment⁶⁰. Similar conclusion may also be drawn for the disc-shaped nanowire quantum dots (which are however not placed on the wetting layer). While we have obtained this characteristic spectra in our earlier work¹¹, we have attributed it the quantum dot shape. In this paper, I demonstrate that strain,

rather than shape only, is responsible for the typical spectra of the disc type quantum dots. Additionally, it is actually the strain that also leads to the characteristic harmonic-oscillator-like structure of confined holes states in lens type InAs/InP quantum dot as seen on Fig. 3 g) and Fig. 10, where no shell-like structure could be observed with strain effects artificially neglected [Fig.3 e) and Fig.8]. Strain cannot be neglected even for InAs/InP quantum dots, commonly considered „low-strain” systems.

Holes states properties may vary significantly in the considered range of VBO values, as $VBO = 0$ means no confinement other than due to strain and material properties („effective mass”) discontinuity (Fig. 9). For small VBO values (and lesser confinement) there is a significant leakage of the hole wavefunction into the surrounding matrix and into the highly biaxially strained wetting layer [Fig. 9 and Fig. 10]. Strained disc type quantum dots reveal thus strong dependence on the choice of valence band offset, however for $VBO > 300$ meV their spectral properties stabilize.

Higher lying holes states have mixed angular momentum character and their evolution with respect to the VBO seems to depend in a complicated way on the relative evolution of different angular momenta components. In terms of states localization I can label hole states by those localized predominately along one of two non-equivalent direction $[110]$ and $[\bar{1}\bar{1}0]$ axis correspondingly. These two species seem to evolve differently under the VBO change, leading to observed ”levels crossings” [Fig. 2 g) and h)]. It is important to reiterate at this point that modification of the VBO is ”artificial”, yet it should be also noticed that it constitutes a very interesting theoretical tool.

E. Strained valence band offset

As expected, InAs/GaAs systems are affected by strain effects more than InAs/InP due to the large lattice mismatch of the former. For a small value of $VBO = 50\text{meV}$, the confining potential for holes is dominated by the strain contribution and the character (anisotropy) of this term leads to the ground (and the first excited) hole state of the apparent, yet unusual p-like symmetry (Fig. 10). I demonstrate results of the calculations for the particularly low (50 meV) VBO value as this number is customarily „used” in the empirical pseudopotential method (EPM^{21,22}). However, I point that it is the strained band offset (being the „combination” of both VBO and a_v valence band deformation potential) that „enters” the calculation

as the actual hole confining potential¹⁴. While the „natural”, i.e., strain free VBO and a_v differ significantly between two methods (ETB: $a_v = 1$ eV and EPM: $a_v = -1$ eV), importantly, the strained band offset obtained by using two sets of a_v and VBO parameters is very similar ≈ 330 meV²⁴. This is illustrated on Figure 11 showing the confining potential profiles calculated for a InAs/GaAs lens type dot using the Bir-Pikus model⁴⁶. This plot was obtained utilizing two sets of parameters: the „recommended” ones from the review paper by Vurgaftman et al.²⁶ ($a_v = +1.0$ eV, VBO = 0.21 eV) and those reported²¹ by the EPM method ($a_v = -1.0$ eV, VBO = 0.05 eV). Thus, in result, the effective confining potentials in the ETB and the EPM approaches are quite similar despite noticeably different bulk (“intermediate”) target values. A more quantitative comparison of the quantum dot results obtained by the ETB and EPM was presented in our recent work¹⁴.

The main difference between the lens type and disc type quantum dots comes from the fact that disc type quantum dots are subject to “smooth”, slowly spatially varying strain (Fig. 12), which also induces uniform heavy hole-light hole splitting leading to single particle like description of hole states. On the contrary, the lens type quantum dots are affected by spatially fluctuating strain due to the curved shape of the quantum dots and the presence of jagged, step-like material interface (Fig 12). Electron states are built predominately from s-type atomic orbitals and are affected only (in the Bir-Pikus formalism^{46,57,58}) by the hydrostatic strain ($Tr(\epsilon) = \epsilon_{xx} + \epsilon_{yy} + \epsilon_{zz}$), that leads predominantly to simple energetic upward shift due to bond lengths deformation in the strained system. Thus electron states are less affected by highly spatially variable biaxial strain.

On the contrary, heavy-holes confining potential (again in the Bir-Pikus formalism) along growth ([001]) quantum dot axis going through the dot center, is given as⁴⁶: $E_{HH} = a_v Tr(\epsilon) - bB(\epsilon)$, where $B(\epsilon) = \epsilon_{zz} - (\epsilon_{xx} + \epsilon_{yy})/2$ is the biaxial component of strain, a_v absolute valence band deformation potential and b is biaxial deformation potential ($b_{InAs} = -1.8$ eV²⁶). Thus, for hole states, the strain related potential shift is an interplay between the hydrostatic and biaxial strain, i.e. the biaxial strain ($-bB(\epsilon) > 0$) deepens the confinement for holes, the hydrostatic strain shallows the confining well in the dot region ($a_v Tr(\epsilon) < 0$).

Fig.13 shows the heavy-hole (in-plane) confining potential (obtained with bulk parameters from ref.²⁶) calculated for all quantum dots considered in this work. For the lens type InAs/GaAs quantum dot one can notice non-regular, “jittered” spatial dependence that will

contribute to the splittings in the shell structure seen in the earlier part of the paper. These oscillations reach up to 50 meV and even lead to formation of attracting well for holes at the edge of quantum dot. This situation is further complicated at the interface as the biaxial strain changes sign⁴⁶ and reverses light-heavy hole ordering, thus affecting the valence band mixing. The interface related oscillation seems to play a small role for the relatively „low-strain” and high VBO value InAs/InP lens type quantum dots, yet it is the complicated character of strain that actually makes the lens type InAs/GaAs holes spectra so different from other quantum dots.

This peculiarity leads, e.g., to the non-Aufbau hole charging pattern and been confirmed by the experiment^{37,38}, the well-established EPM and also recent k.p calculations³⁵. It is only for quite large²⁶ InAs/GaAs VBO values (> 0.450 eV) that hole charge distributions of lens type quantum dot resemble [Fig. 10] that of the harmonic oscillator-like states. However even for $VBO > 0.7$ eV the hole p-states splitting does not drop below 5 meV. One can expect this effect should be more pronounced in tall lens, cones or pyramid type (high aspect ratio⁷) quantum dots³⁵.

If accurate (order of meV’s) modeling of hole states is important, then the choice of the „natural” VBO plays an important role. This is particularly noticeable for lens type InAs/GaAs quantum dot [Fig. 3]. In the ”recommended” range of VBO values²⁶ (210 – 350 meV), hole $h_1 - h_2$ level spacing varies between 9 meV and 14 meV and spacings of higher lying level change even more substantially, e.g. $h_3 - h_4$ spacing varies from 1 meV to 7 meV.

IV. MANY-BODY STATES

Strain effects and the valence band offset play a fundamental role for the single particle states in quantum dots. Next, I calculate many-body properties of single exciton and excitonic complexes.

A. Exciton fine structure

Fig. 14 shows excitonic fine structure⁶¹ calculated for different VBO values for lens and disc type InAs/GaAs and InAs/InP quantum dots. The energy difference between the two

bright excitonic states, the so called bright exciton splitting (BES), is related to the confining potential anisotropy⁶¹. The BES is thus larger for curved-shape, highly anisotropic, lens type quantum dots, reaching values varying between 40 – 60 meV, while for disc type quantum dots the BES does not exceed 20 meV. These results are in quantitative agreement with recent EPM calculations⁴⁴, however as noticed by the EPM researchers⁶² this method systematically predicts much lower BES value than those reported in the experiment (or in current ETB work).

For lens type quantum dots the BES varies noticeably with respect to the VBO value, while it has almost flat VBO dependence for disc shaped systems. While Fig. 14 is the result of the full many-body configuration interaction calculation¹², including single particle states up to the d-shell, the majority of the BES splitting and the overall trend is very well reproduced (not shown here) by a single electron-hole anisotropic exchange (complex) integral^{4,12,15,61}:

$$V_{eh}^{b-b} \equiv V_{e_{\uparrow}h_{\downarrow}e_{\downarrow}h_{\uparrow}} = \int \int \frac{e_{\uparrow}(\mathbf{r})^* h_{\downarrow}(\mathbf{r}')^* e_{\downarrow}(\mathbf{r}') h_{\uparrow}(\mathbf{r})}{\epsilon(\mathbf{r}, \mathbf{r}') |\mathbf{r} - \mathbf{r}'|} d\mathbf{r} d\mathbf{r}',$$

where $\epsilon(\vec{r}_1, \vec{r}_2)$ is the position-dependent dielectric function, (e) electron and (h) hole are in their ground s-states and arrows correspond to carrier quasi-spins. V_{eh}^{b-b} (as all other Coulomb matrix elements in this work) is calculated using Eq. 3.

V_{eh}^{b-b} is responsible for mixing of two bright excitonic states ($\uparrow\downarrow$ and $\downarrow\uparrow$) and therefore leads to the BES. The BES is thus a two-body effect of the s-shell electron and hole spatial anisotropy and as such is not directly correlated with the electron p-shell splitting/anisotropy (Fig. 5).

The BES is larger for highly strained lens type InAs/GaAs quantum dot (Fig. 14), as the low symmetry (C_{2v}) of the confining potential is clearly related to strain²⁰. On the other hand the electron-hole anisotropic exchange interaction is also related to the electron-hole "overlap" in V_{eh}^{b-b} . Therefore, similar confinement of electron and hole may lead to larger BES. Thus, for low strain InAs/InP disc type quantum dot, where electron and hole charge distributions ("envelopes") are almost identical (as seen previously on Fig.4 and Fig.9), the BES value ($\approx 18\mu\text{eV}$) is almost two times larger than for highly strain InAs/GaAs disc type quantum dot ($\approx 8\mu\text{eV}$). This is in clear contradiction to the recent EPM calculations⁶³, which predict highly reduced fine-structure splitting in InAs/InP quantum dots. Finally, should the wetting layer be neglected the BES for disc type quantum dots would be exactly

zero due to high (D_2d) overall (lattice and shape) quantum dot symmetry⁴⁴. To summarize, the BES is a non-trivial function of quantum dot shape, shape and quantum dot/matrix materials.

The dark-bright exchange splitting is determined predominantly by a (real) exchange matrix element which also conserves spin (V_{eh}^{d-b}). The bright-dark exciton splitting does not vary significantly with VBO: increased confinement of hole seems to be assisted by the decreased confinement of electron, and the overall electron-hole exchange integral and dark-bright exciton splitting does not vary too much. Based on similar arguments as for the BES, the bright-dark exciton splitting for disc type quantum dots is generally larger than for lens type quantum dots. Additionally bright-dark exciton splitting will be larger for cases with better electron-hole overlap: InAs/GaAs rather than InAs/InP disc type quantum dot and InAs/InP rather than InAs/GaAs lens type quantum dot.

Finally, the dark exciton splitting is a pronounced and complicated function of the VBO, especially for InAs/GaAs systems, varying over an order of magnitude for the studied VBOs. Dark exciton splitting is generally larger for smaller VBO value, however no clear trend regarding the matrix material is observed.

B. XX , X^- and X^+ binding energies

Fig. 15 shows biexciton (XX) and charged trions (X^- and X^+) binding energies, measured with respect to the single exciton energy ($E_B^{XX} = E^{XX} - E^X$, $E_B^{X^-} = E^{X^-} - E^X$, etc.), for different VBO values for lens and disc type InAs/GaAs and InAs/InP quantum dots.

For InAs/GaAs lens type quantum dot, the biexciton binding energy varies significantly and even changes its sign at $VBO \approx 170$ meV, leading to the unbound biexciton for $VBO < 170$ meV. Similarly for this system, binding energies of charged excitons vary over large range of values, with bound to unbound transition for X^- at $VBO \approx 0.35$ eV. For InAs/InP lens type quantum dot, in the "realistic"²⁶⁻³³ range of InAs/InP VBO values (300 – 400 meV), charged complexes even reverse their relative position in a complicated way, e.g. for $VBO = 0.3$ eV, one observes the following ordering of spectral lines with the increasing energy: XX , X^+ , X^- , X , while for $VBO \approx 0.4$ the order of lines is following: X^- , XX , X^+ , X . For InAs/GaAs disc type quantum dot ("realistic"²⁶⁻³³ $VBO \approx 200 - 300$ meV), one observes following order of spectral lines: X^- , XX , X^+ and X , while for InAs/InP disc

type quantum dots (VBO $\approx 300 - 400$ meV) one gets: X^- , XX , X and X^+ . In all considered cases absolute binding energies and relative order of spectral lines depend significantly on the VBO, quantum dot shape and substrate material. And thus caution should be exercised when applying different VBO values in excitonic calculations.

Binding energies must be calculated using the full many-body approach^{24,55,64}:

$$\begin{aligned} E_B^{XX} &= J_{ss}^{ee} + J_{ss}^{hh} - 2J_{ss}^{eh} - \Delta E_{corr}^{XX} \\ E_B^{X^-} &= J_{ss}^{ee} - J_{ss}^{eh} - \Delta E_{corr}^{X^-} \\ E_B^{X^+} &= J_{ss}^{hh} - J_{ss}^{eh} - \Delta E_{corr}^{X^+} \end{aligned}$$

where electron-electron (J_{ee}), hole-hole (J_{hh}) and electron-hole J_{eh} Coulomb integrals are calculated for electron and hole occupying the s-shell ground states, while the important correction due to correlation effects ΔE_{corr} can be attributed to the configuration mixing effects with higher lying states. In the Hartree-Fock approximation $\Delta E_{corr} = 0$, while realistic values of binding energies ($\Delta E_{corr} \neq 0$) can be calculated using the full configuration interaction method^{24,55,64}.

For example, for lens type InAs/GaAs quantum dot, for the VBO= 0.1 eV, $J_{ee} = 26.28$ meV, $J_{eh} = 19.54$ meV and at the level of Hartree-Fock (perturbation theory) approximation X^- binding energy can be calculated as $\Delta E^{HF}(X^-) = J_{ss}^{ee} - J_{ss}^{eh} = 6.75$ meV. This value is further reduced by the correlation correction $\Delta E_{corr}^{X^-} = 1.41$ meV and therefore finally $E_B^{X^-} = 5.34$ meV. On the other hand, for VBO= 0.5 meV $J_{ee} = 20.88$ meV, $J_{eh} = 21.68$ meV, leading to $\Delta E^{HF}(X^-) = -0.8$ meV. The CI calculated correlation correction is $\Delta E_{corr}^{X^-} = 1.52$ meV and thus we obtain $E_B^{X^-} = -2.32$ meV.

The correction due to correlation mixing is important (≈ 1.5 meV) and cannot be neglected, however its value does change significantly as the VBO is varied. In the previous section I discussed that while the absolute values of excitonic fine structure splittings were results of the full configuration interaction procedure, the observed trends could be analyzed in terms of single exchange integral. Quite similar situation takes also place for the excitonic complexes binding energies. The absolute value of the binding energy must be calculated using the many body approach, yet its evolution with respect to the VBO can be understood at the level of Hartree-Fock (perturbation theory) approximation and several s-shell electron-hole Coulomb integrals (J_{ee} , J_{eh} and J_{hh}), while the correlation correction ΔE_{corr} is virtually unaffected by the choice of the VBO.

V. SUMMARY

Valence band offset is one of the important empirical parameters for the semi-empirical tight-binding method. By a thorough VBO analysis I have shown a non-trivial interplay between confinement potential due to the band offset and confinement due to strain. With strain effects artificially neglected, no shell structure for holes is present, with complicated charge density distribution due to light and heavy hole band mixing effects. With strain effects included, heavy holes and light holes are decoupled from each other by the biaxial strain and the shell-like structure characteristic for single band models is restored. Notable difference from this picture is observed for the strained InAs/GaAs lens type quantum dot. Due to anisotropy and inhomogeneity of strained induced confining potential splittings of excited hole states dominate over shell spacings, even for the largest considered VBO value. Peculiar structure of hole levels in InAs/GaAs in lens type QDs, so much different from InAs/InP QDs, origins thus from strain and not due to the different VBO as suggested by the other studies²³. On the other hand the characteristic shell structure of InAs/GaAs disc type QDs or InAs/InP lens type QDs also origins from strain effects. In all considered cases, even for "low-strain" InAs/InP systems, strain effects and large VBO value lead to spectral structure of hole levels known from experimental results. Therefore, strain cannot be neglected even in nominally "low-strain" InAs/InP quantum dots, whether disc or lens shaped.

Valence band offset also affects many body properties such as excitonic fine structure and binding energies of excitonic complexes. Exciton fine structure splittings values reported in this work are much larger than those reported by the EPM and thus much closer to the experimentally reported values without the necessity of inclusion of the "ordering" effects⁶². Fine structure splitting is also shown to vary depending on the matrix material (InP/GaAs) and the inclusion of strain. Charged excitons and biexciton binding energies vary strongly on the depth of confinement potential (VBO) with clear distinction from the simple effective mass ("harmonic oscillator") picture. This should be emphasized as the reliable prediction of excitonic binding energies is of key importance for so-called "inverse approaches"⁴³.

The paper studies differences between flat („indium flushed”) and lens type quantum dots, the relation between hydrostatic and biaxial strain in these systems, and quantitatively estimates the role of a jagged quantum dot/matrix material interface. The paper shows that

the unrealistic p-shell symmetry of ground hole state would be obtained if ETB used the VBO value taken directly from the EPM and then discusses differences and similarities (“strained band offset”) between both approaches. Finally the paper shows that the VBO is not merely a technological parameter, and the caution should be exercised when applying different VBO values.

VI. ACKNOWLEDGEMENTS

This work was supported by the Foundation for Polish Science, Homing Plus Programme co-financed by the European Union within the European Regional Development Fund. The author would like to thank G. W. Bryant, W. Jaskólski, and E. Kadantsev for discussions and careful reading of the manuscript.

* Electronic address: mzielin@fizyka.umk.pl

- ¹ L. Jacak, P. Hawrylak, and A. Wojs, *Quantum Dots* (Springer, Berlin, 1998).
- ² M. T. Bjork et al., *Nano Letters* **4**, 1621, (2004).
- ³ S. Schulz, S. Schumacher, and G. Czycholl, *Phys. Rev. B* **73**, 245327 (2006).
- ⁴ S. Lee, L. Jönsson, J.W. Wilkins, G.W. Bryant, and G. Klimeck, *Phys. Rev. B* **63**, 195318 (2001).
- ⁵ K. Leung and K.B. Whaley, *Phys. Rev. B* **56**, 7455 (1997).
- ⁶ J.G. Diaz and G.W. Bryant, *Phys. Rev. B* **73**, 075329 (2006).
- ⁷ M. Usman, *Phys. Rev. B* **86**, 155444 (2012).
- ⁸ M. Usman, *J. Appl. Phys.* **110**, 094512 (2011).
- ⁹ R. Santoprete, B. Koiller, R. B. Capaz, P. Kratzer, Q. K. K. Liu, and M. Scheffler, *Phys. Rev. B* **68**, 235311 (2003).
- ¹⁰ W. Jaskólski, M. Zieliński, G.W. Bryant, and J. Aizpurua, *Phys. Rev. B* **74**, 195339 (2006).
- ¹¹ M. Korkusiński, M. Zieliński, and P. Hawrylak *J. Appl. Phys.* **105**, 122406 (2009).
- ¹² M. Zielinski, M. Korkusinski, and P. Hawrylak, *Phys. Rev. B* **81**, 085301 (2010).
- ¹³ W. Sheng, S.-J. Cheng, and P. Hawrylak, *Phys. Rev. B* **71**, 035316 (2005).
- ¹⁴ M. Zielinski, *Phys. Rev. B* **86** 115424 (2012).

- ¹⁵ G. W. Bryant et al., Phys Rev Lett. **105**, 067404 (2010).
- ¹⁶ G. W. Bryant et al., Phys. Rev. B **84**, 235412 (2011).
- ¹⁷ L. W. Wang and A. Zunger, Phys. Rev. B **59**, 15806 (1999).
- ¹⁸ L. W. Wang, A. J. Williamson, Alex Zunger, H. Jiang, and J. Singh, Appl. Phys. Lett. **76**, 339 (2000).
- ¹⁹ A. Canning, L.W. Wang, A. Williamson, and A. Zunger J. Comp. Phys. **160**, 29 (2000).
- ²⁰ G. Bester and A. Zunger, Phys. Rev. B **71**, 045318 (2005).
- ²¹ L. He and A. Zunger Phys. Rev. B **73**, 115324 (2006).
- ²² A. J. Williamson, L. W. Wang, and A. Zunger Phys. Rev. B **62**, 12963 (2000).
- ²³ M. Gong, K. Duan, Ch.-F. Li, R. Magri, G. A. Narvaez, and L. He, Phys. Rev B **77**, 045326 (2008).
- ²⁴ M. Gong M, W. Zhang, G. Can Guo G, and L. He Appl. Phys. Lett. **99**, 231106 (2011).
- ²⁵ J.M. Jancu, R. Scholz, F. Beltram, and F. Bassani, Phys. Rev. B **57**, 6493 (1998).
- ²⁶ I. Vurgaftman and J. R. Meyer, W L. R. Ram-Mohan Appl. Phys. Rev. **89**, 5815 (2001).
Please note that ref.²⁶ uses sign convention for a_v different from many other works found in the literature.
- ²⁷ Y.H. Li, and X.G. Gong, S.H. Wei, Phys. Rev. B **73**, 245206 (2006).
- ²⁸ S.H. Wei and A. Zunger, Phys. Rev. B **60**, 5404 (1999).
- ²⁹ Chris G. Van de Walle, Phys. Rev. B **39**, 1871 (1989).
- ³⁰ Kent, Hart, Zunger, Appl. Phys. Lettt 81, 4377 (2002)
- ³¹ E S. Kadantsev, M. Zielinski, Marek Korkusinski, and Pawel Hawrylak, J. Appl. Phys. **107**, 104315 (2010).
- ³² E S. Kadantsev, M. Zielinski, and Pawel Hawrylak, Phys. Rev. B **86**, 085411 (2012).
- ³³ E.S. Kadantsev and P. Hawrylak, Appl. Phys. Lett. **98**, 023108 (2011).
- ³⁴ Y.-H. Li, A. Walsh, A. S. Chen, W.-J. Yin, J.-H. Yang, J. Li, J. L. F. Da Silva, X. G. Gong, and S.-H. Wei Appl. Phys. Lett. **94**, 212109 (2009).
- ³⁵ A. Schliwa, M. Winkelnkemper, and D. Bimberg Phys. Rev. B **76**, 205324 (2007).
- ³⁶ T.B. Boykin, G. Klimeck, R.C. Bowen, and F. Oyafuso, Phys. Rev. B **66**, 125207 (2002).
- ³⁷ J.H. Blokland et al., Phys. Rev. B **75**, 233305 (2007).
- ³⁸ M. Ediger, G. Bester, A. Badolato, P. M. Petroff, K. Karrai, A. Zunger, R. J. Warburton Nature Physics **3**, 774 (2007).

- ³⁹ O. Benson, C. Santori, M. Pelton, and Y. Yamamoto Phys. Rev. Lett. **84**, 2513 (2000).
- ⁴⁰ J. E. Avron et al., Phys. Rev. Lett. **100**, 120501 (2008).
- ⁴¹ F. Ding et al., Phys. Rev. Lett. **104**, 067405 (2010).
- ⁴² M. E. Reimer et al., Nano Lett. **11**, 645 (2011).
- ⁴³ V. Mlinar, M. Bozkurt, J. M. Ulloa, M. Ediger, G. Bester, A. Badolato, P. M. Koenraad, R. J. Warburton, A. Zunger, Phys. Rev. B **80**, 165425 (2009).
- ⁴⁴ R. Singh and G. Bester, Phys. Rev. Lett. **103**, 063601 (2009).
- ⁴⁵ P.N. Keating, Phys. Rev. **145**, 637 (1966); R.M. Martin, Phys. Rev. B **1**, 4005 (1970).
- ⁴⁶ C. Pryor, J. Kim, L.W. Wang, A.J. Williamson, and A. Zunger, J. Appl. Phys. **83**, 2548 (1998).
- ⁴⁷ T. Saito, Y. Arakawa, Physica E **15**, 169 (2002).
- ⁴⁸ M. Zielinski, Acta Phys. Pol. A, **122**, 312 (2012).
- ⁴⁹ G. Bester, A. Zunger, X. Wu, and D. Vanderbilt, Phys. Rev. B **74**, 081305 (2006).
- ⁵⁰ D.J. Chadi, Phys. Rev. B **16**, 790 (1977).
- ⁵¹ S. Lee, F. Oyafuso, P. von Allmen, and G. Klimeck Phys. Rev. B **69**, 045316 (2004).
- ⁵² G. Onida, L. Reining, A. Rubio, Rev. Mod. Phys. **74**, 601 (2002).
- ⁵³ P. Hawrylak and M. Korkusinski, in: *Single Quantum Dots: Fundamentals, Applications, and New Concepts*, P. Michler (Ed.), *Topics in Applied Physics*, vol. 90, Springer, 2003.
- ⁵⁴ Y.-M. Niquet, Ch. Delerue, Phys. Rev. B **84**, 075478 (2011).
- ⁵⁵ A. Wojs, P. Hawrylak, S. Fafard, and L. Jacak, Phys. Rev. B **54**, 5604 (1996).
- ⁵⁶ E.O. Kande, Journal of Physics and Chemistry of Solids, 1 (4), 249, (1957).
- ⁵⁷ G. L. Bir and G. E. Pikus, *Symmetry and Strain-Induced Effects in Semiconductors* (Wiley, New York, 1975).
- ⁵⁸ P.Y. Yu and M. Cardona, *Fundamentals of Semiconductors: Physics and Materials Properties* (Springer, Berlin, 2005).
- ⁵⁹ Z. R. Wasilewski, S. Fafard, and J. P. McCaffrey, J. Cryst. Growth **201202**, 1131 (1999).
- ⁶⁰ S. Raymond, S. Studenikin, A. Sachrajda, Z. Wasilewski, S. J. Cheng, W. Sheng, P. Hawrylak, A. Babinski, M. Potemski, G. Ortner, and M. Bayer, Phys. Rev. Lett. **92**, 187402 (2004).
- ⁶¹ M. Bayer et al., Phys. Rev. B **65**, 195315 (2002).
- ⁶² R. Singh and G. Bester, Phys. Rev. B **84**, 241402(R) (2011).
- ⁶³ L. He, M. Gong, C-F Li, G-C Guo, and A. Zunger Phys. Rev. Lett. **101**, 157405 (2008).
- ⁶⁴ M. Zielinski, Nanoscale Research Letters **7**, 265 (2012).

⁶⁵ Incorporation of piezoelectricity, necessarily for high aspect ratio (tall) quantum dots, would further complicate that picture.

⁶⁶ While the reported InAs/GaAs VBO extreme values vary from 60 meV to 500 meV, the more "realistic" or the "recommended"²⁶ values can be limited to narrower range.

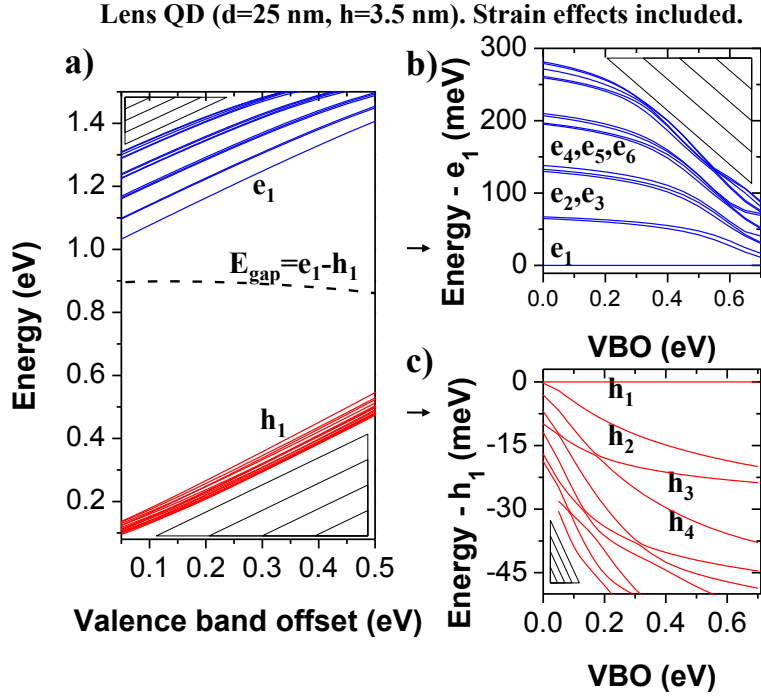


FIG. 1: (Color online) Single particle (electron and hole) energies (a) and effective gap $E_{gap} = e_1 - h_1$ for InAs/GaAs lens type (d=25 nm, h=3.5 nm) quantum dot as a function of quantum dot (InAs) and matrix (GaAs) valence band offset (VBO). Single particle electron (b) and hole (c) energies are calculated with respect to electron (e_1) and hole (h_1) ground states energies. Patterned areas mark higher, excited states.

Disc type QD (d=16.8 nm, h=3 nm).

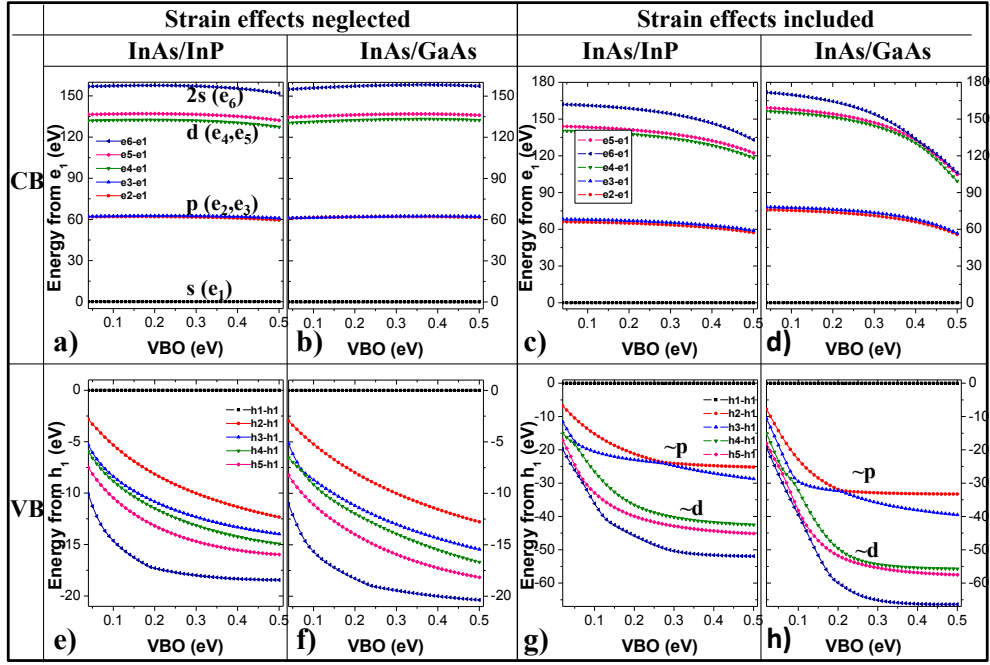


FIG. 2: Electron (conduction band - CB) and hole (valence band - VB) single particle energies calculated with respect to electron and hole ground states energies (e_1 and h_1 correspondingly) for InAs/InP and InAs/GaAs disc type (d=16.8 nm, h=3 nm) quantum dots as a function of quantum dot (InAs) and matrix (GaAs or InP) valence band offset (VBO). Strain-effects are either included or artificially neglected.

Lens type QD ($d=25$ nm, $h=3.5$ nm).

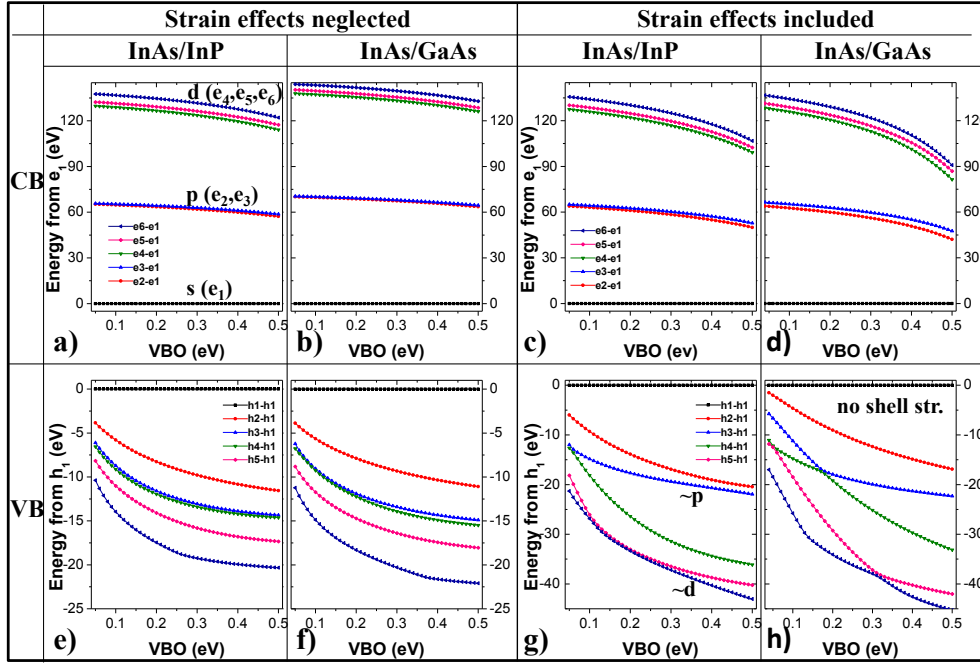


FIG. 3: Electron (conduction band - CB) and hole (valence band - VB) single particle energies calculated with respect to electron and hole ground states energies (e_1 and h_1 correspondingly) for InAs/InP and InAs/GaAs lens type ($d=25$ nm, $h=3.5$ nm) quantum dots as a function of quantum dot (InAs) and matrix (GaAs or InP) valence band offset (VBO). Strain-effects are either included or artificially neglected.

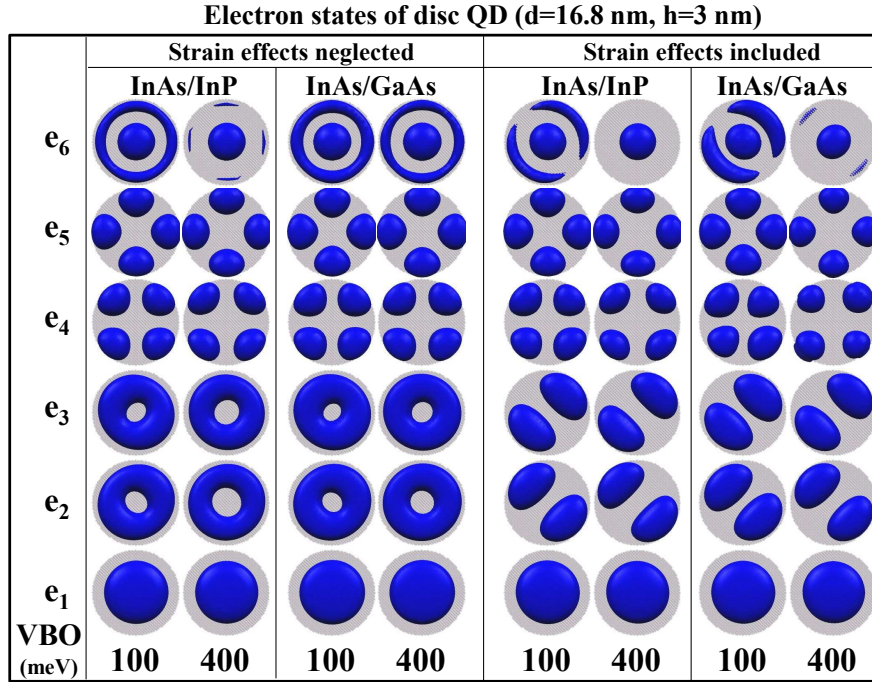


FIG. 4: Electron probability density isosurfaces for InAs/InP and InAs/GaAs disc type (d=16.8 nm, h=3 nm) quantum dots as a function of quantum dot (InAs) and matrix (GaAs or InP) valence band offset (VBO). Strain-effects are either included or artificially neglected.

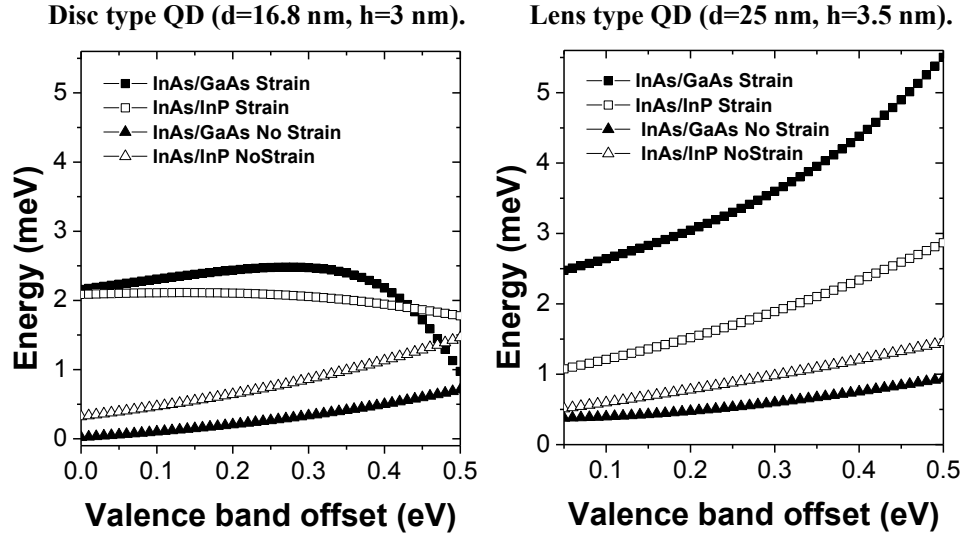


FIG. 5: Splitting of the electron p-shell calculated for InAs quantum dots of different shape, matrix material and as a function of quantum dot (InAs) and matrix (GaAs or InP) valence band offset (VBO).

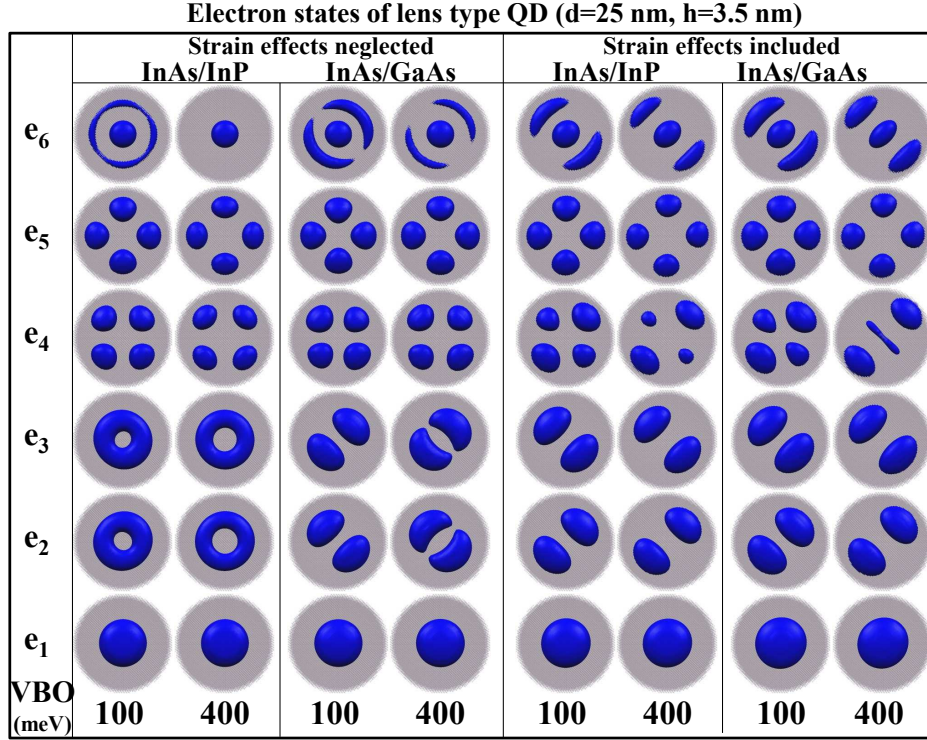


FIG. 6: Electron probability density isosurfaces in InAs/InP and InAs/GaAs lens type ($d=25$ nm, $h=3.5$ nm) quantum dots as a function of quantum dot (InAs) and matrix (GaAs or InP) valence band offset (VBO). Strain-effects are either included or artificially neglected.

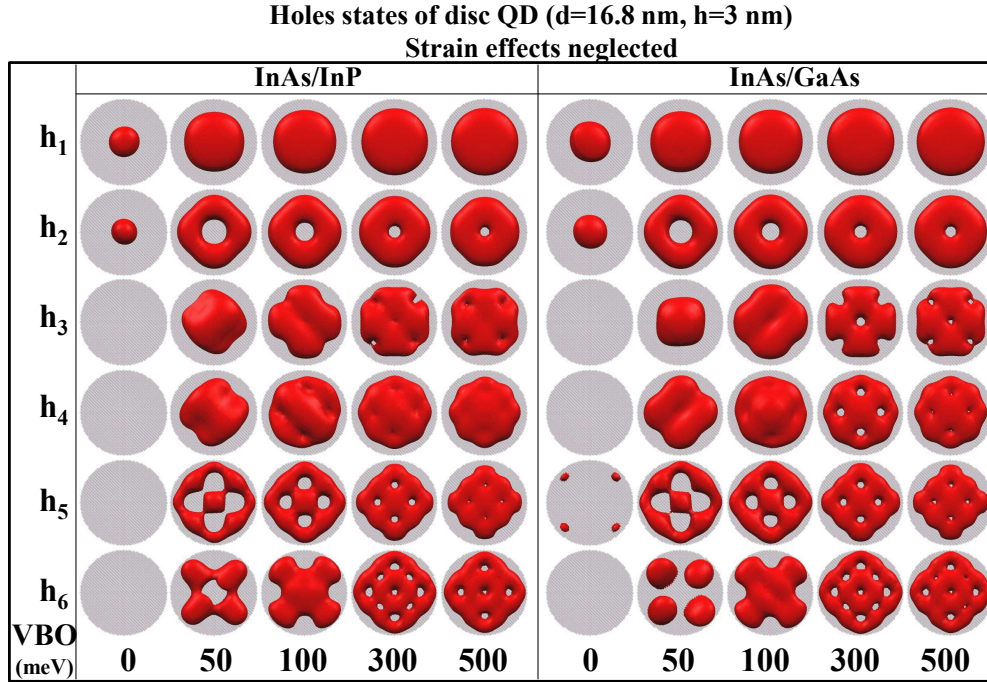


FIG. 7: Hole probability density isosurfaces in InAs/InP and InAs/GaAs disc type (d=16.8 nm, h=3 nm) quantum dots as a function of quantum dot (InAs) and matrix (GaAs or InP) valence band offset (VBO). Strain-effects are artificially neglected.

Hole states of lens type QD ($d=25$ nm, $h=3.5$ nm). Strain effects neglected.

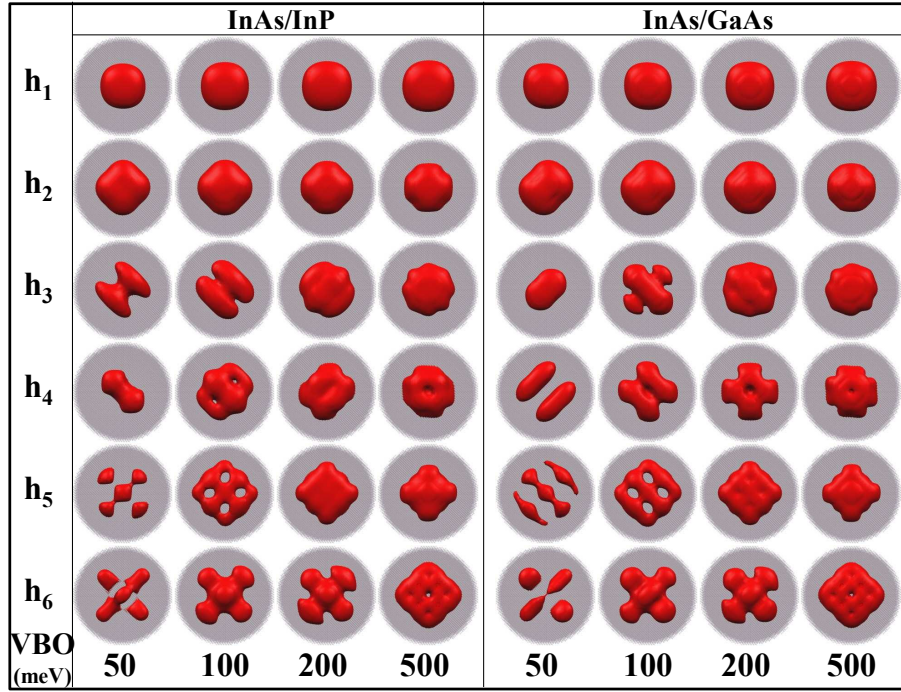


FIG. 8: Hole probability density isosurfaces in InAs/InP and InAs/GaAs lens type ($d=25$ nm, $h=3.5$ nm) quantum dots as a function of quantum dot (InAs) and matrix (GaAs or InP) valence band offset (VBO). Strain-effects are artificially neglected.

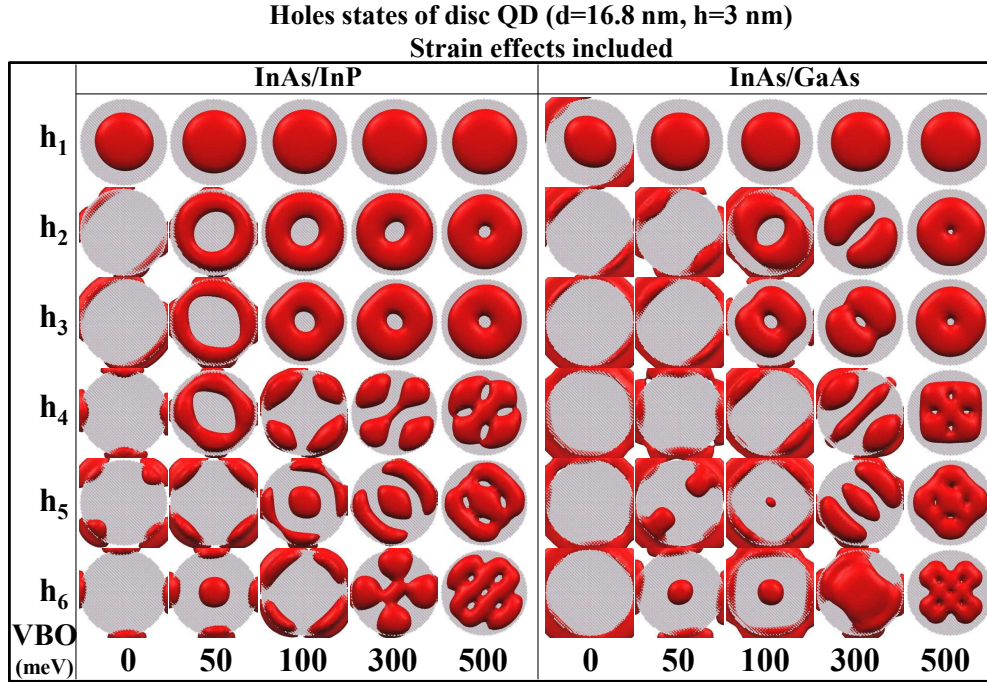


FIG. 9: Hole probability density isosurfaces in InAs/InP and InAs/GaAs disc type (d=16.8 nm, h=3 nm) quantum dots as a function of quantum dot (InAs) and matrix (GaAs or InP) valence band offset (VBO). Strain-effects are included.

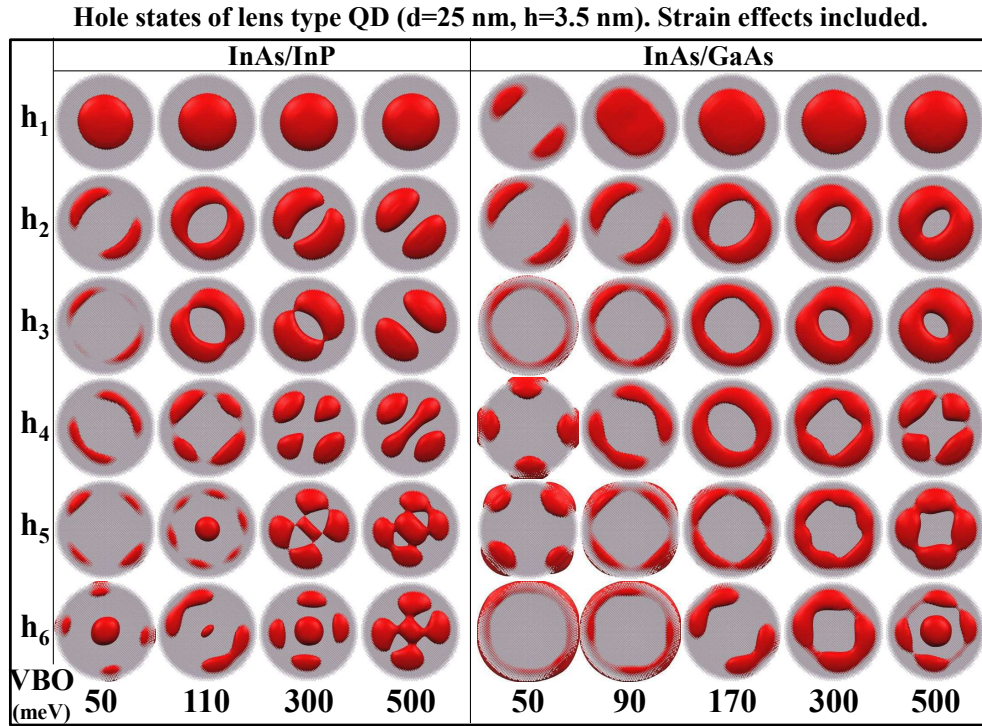


FIG. 10: Hole probability density isosurfaces in InAs/InP and InAs/GaAs lens type (d=25 nm, h=3.5 nm) quantum dots as a function of quantum dot (InAs) and matrix (GaAs or InP) valence band offset (VBO). Strain-effects are included.

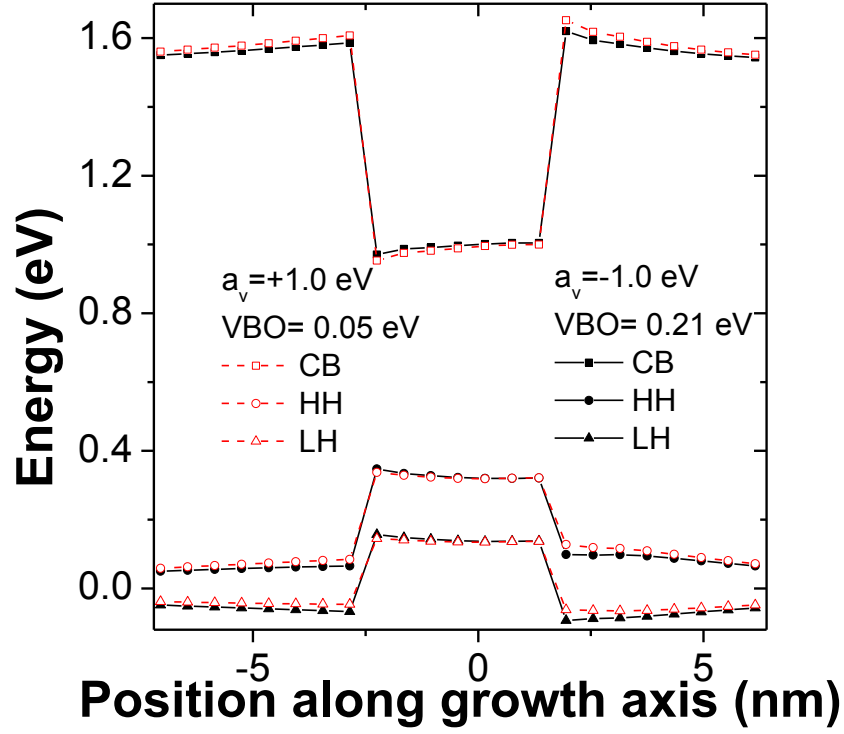


FIG. 11: Strain-induced confining potentials for a InAs/GaAs lens type ($d=25$ nm, $h=3.5$ nm) quantum dot along [001] axis, calculated using the Bir-Pikus model and two sets of bulk VBO and a_v parameters. Conduction band (CB) - squares, heavy-hole band (HH) - circles, light-hole band (LH) - triangles.

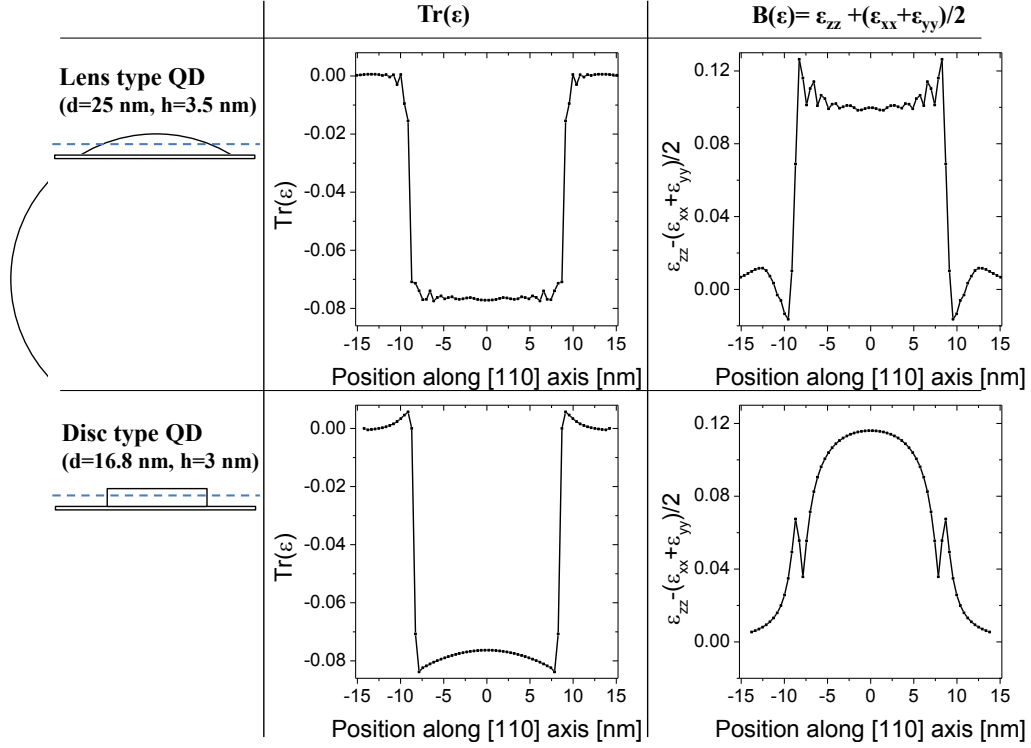


FIG. 12: Trace $Tr(\epsilon)$ of the strain tensor and the biaxial $B(\epsilon) = \epsilon_{zz} - (\epsilon_{xx} + \epsilon_{yy})/2$ component of strain for a disc type ($d=16.8$ nm, $h=3$ nm) and a lens type ($d=25$ nm, $h=3.5$ nm) InAs/GaAs quantum dot. Profiles has been calculated along $[110]$ direction, $z = 2$ nm from the QD base.

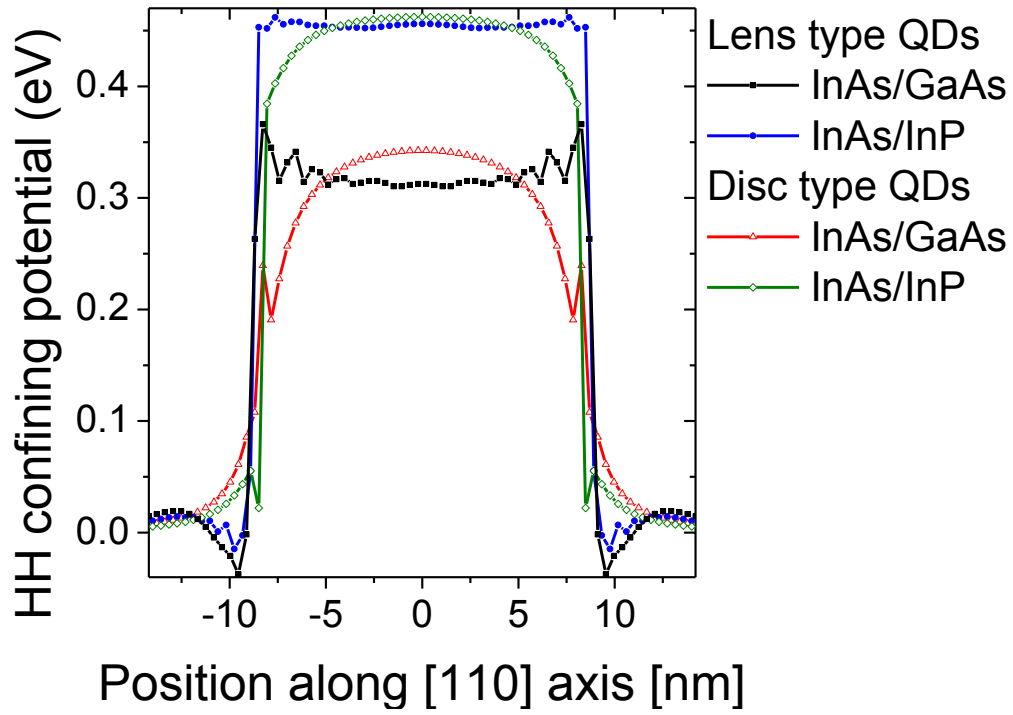


FIG. 13: Strain-induced heavy-hole confining potentials for InAs/GaAs and InAs/InP disc type ($d=16.8$ nm, $h=3$ nm) and lens type ($d=25$ nm, $h=3.5$ nm) quantum dots. Profiles has been calculated using the Bir-Pikus model along [110] direction, $z = 2$ nm from the QD base.

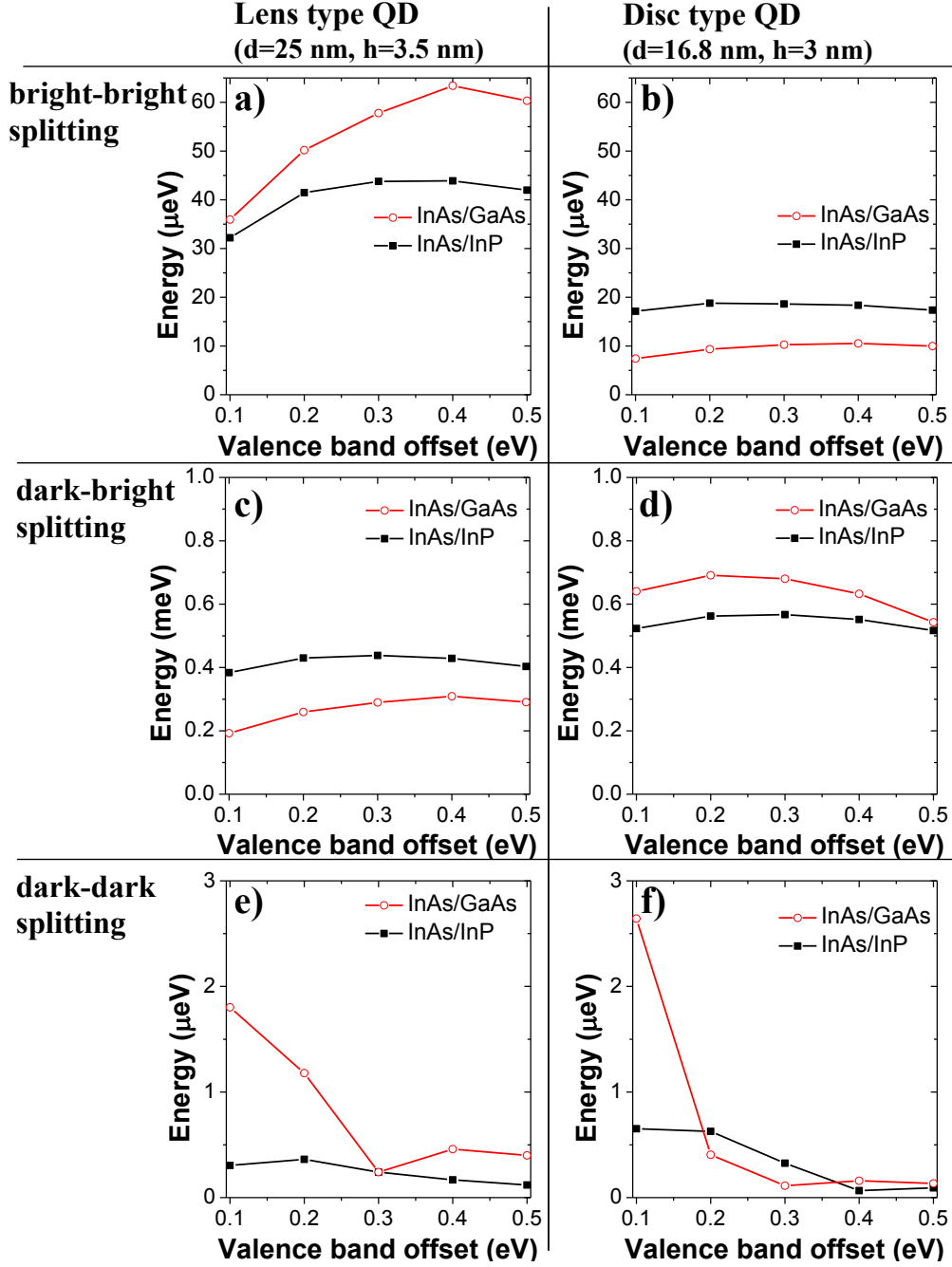


FIG. 14: Excitonic fine structure for InAs/GaAs (open circles) and InAs/InP (squares) disc type ($d=16.8$ nm, $h=3$ nm) and lens type ($d=25$ nm, $h=3.5$ nm) quantum dots as a function of quantum dot (InAs) and matrix (GaAs or InP) valence band offset (VBO).

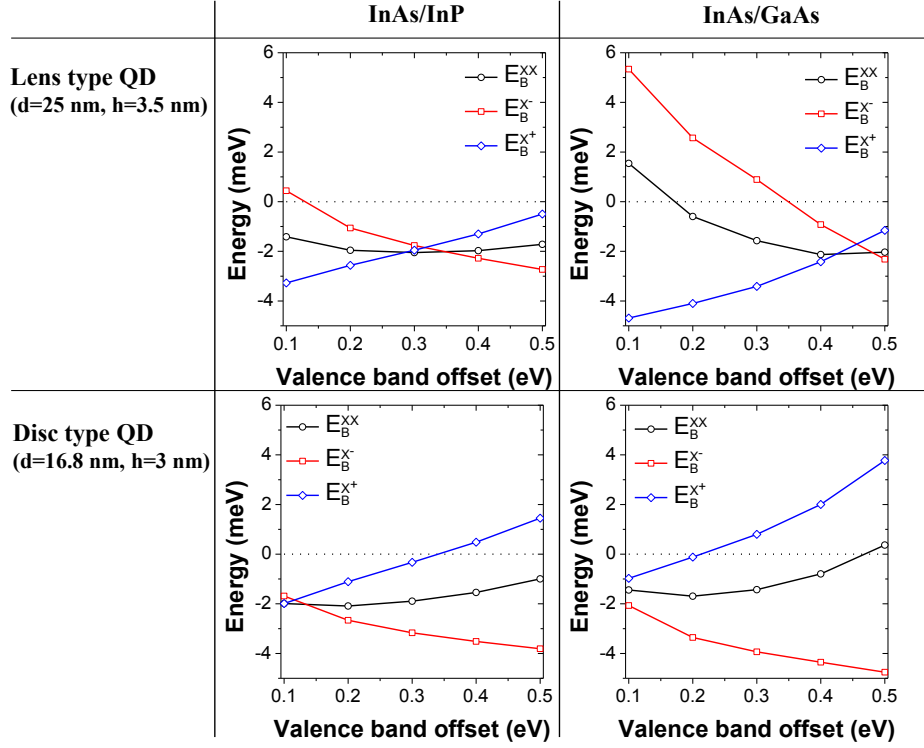


FIG. 15: Biexciton XX (black-circles), negatively charged X^- (red-squares) and positively charged X^+ (blue-diamonds) excitons binding energies, calculated with respect to the single, neutral, exciton energy, for InAs/GaAs and InAs/InP disc type ($d=16.8$ nm, $h=3$ nm) and lens type ($d=25$ nm, $h=3.5$ nm) quantum dots as a function of quantum dot (InAs) and matrix (GaAs or InP) valence band offset (VBO).